



Assessment of land use/land cover changes and their impacts on land surface temperature in Bangui (the capital of Central African Republic)



Mamadou Traore ^{a,*}, Mai Son Lee ^b, Azad Rasul ^c, Abel Balew ^{d,*}

^a Department of Geological Engineering, Çukurova university, 01330 Sarıçam, Adana, Turkey

^b The Graduate Institute of Hydrological and Oceanic Sciences, National Central University, Jhongli, Taoyuan, Taiwan, ROC

^c Department of Geography, Soran University, Kawa Street, Soran 44008, Erbil, Iraq

^d Department of Geography and Environmental Studies, Woldia University, Ethiopia

ARTICLE INFO

Keywords:

Remote sensing
NDBI
NDVI
NDLI
LST

ABSTRACT

Extreme land-use and land-cover (LULC) as the result of rapid urbanization has been raising land surface temperature of core city areas and its surrounding. Therefore, investigation on surface temperature is very vital to analyze temperature variations and minimize its effect. This research aims to analyze the impacts of LULC changes on LST in Bangui city, Central African Republic using combined techniques of remote sensing and GIS. The result of this study indicates that there was a significant change in LULC between 1986 and 2017 particularly expanded in vegetation and built-up areas and declined in bare soil. For instance, built-up increased by + 130.29 % with a rate of 137.06; and vegetation increased by 8.44% or a rate of 17.2. Whereas bare soil was sharply declined by -35.33% for a rate of -155.83. The mean LST of the city firstly decreased from 26.24 °C in 1986 to 23.37 °C in 1999 and increased to 27.23 °C in 2017. The study also stated that the mean LST of built-up areas increased from 26.21 °C in 1986 to 27.59 °C in 2017. Besides, the mean LST of bare soil raised from 26.51 °C to 27.33 °C in 1986 and 2017 respectively. These indicate that built up and bare soil experienced high LST than vegetation and water body. The study found a positive correlation between NDBI and LST whereas negative correlations of LST with NDVI and NDLI. City planners should be implemented urban green belts and green roof to mitigate the effect of surface urban heat islands (SUHI) in the city and its surroundings.

1. Introduction

Currently, many regions around the globe under different environmental conditions are facing dramatic changes in LULC (Solaimani et al., 2010). The primary and significant cause of changes in LULC is mainly associated with rapid urbanization (Kalnay and Cai, 2003; Chen et al., 2006; Omar et al., 2014). Urbanization has become a universal trend under the combined influences of biological factors as well as anthropogenic activities, which plays a vital role in LULC transition of any area (Seto et al., 2011; Sun et al., 2013; Lu et al., 2018). Because an increase in urban population demands metropolitan luxuries, facilities for their livings, and that adverse growth of urbanization cause changes in LULC (Rajeshwari and Mani, 2014; Zhang et al., 2018). In recent eras, because of several natural and anthropoid elements, the land cover has been changed at a large scale mainly forest cover transformed into farmland and settlement (Bounoua et al., 2018; Lu et al., 2019; Mumtaz et al., 2020). Such conversion of land covers to land use have been greatly influencing the eco-environment (Wu and Zhang, 2012), as well as

often threatens the sustainable urban development (Poelmans and Van Rompaey, 2009; Dubovik et al., 2011). Extreme changes of LULC in response to urbanization also causes an increase in surface temperature (Bounoua et al., 2018; Sisay and Korme, 2019; Balew and Korme, 2020). Because, in terms of absorption and radiation of energy, each LULC class has its own unique qualities (Mumtaz, 2020). Many research highlights that artificial changes in LULC such as urbanization, deforestation, and land degradation have a significant impact on the urban ecosystem (Abdullahi and Pradhan, 2018; Bounoua et al., 2018; Lu et al., 2019). These artificial changes in LULC are also the leading cause changes in LST mainly an expansion of impervious surface has a sever impact (Dissanayake et al., 2019a; Ranagalage et al., 2019; Simwanda et al., 2019; Balew and Korme, 2020). LST is one of the main challenges of most cities of the world which resulted from natural disasters and human induces factors mainly LULC changes. The extreme change in LULC raising the effects of SUHI. Therefore, to live friendly within the environment basic alternative solutions and different mitigation strategies should be implemented.

* Corresponding authors.

E-mail addresses: matraba77@gmail.com (M. Traore), lmson2603@gmail.com (M.S. Lee), azad977@gmail.com (A. Rasul), abelbalew@gmail.com (A. Balew).

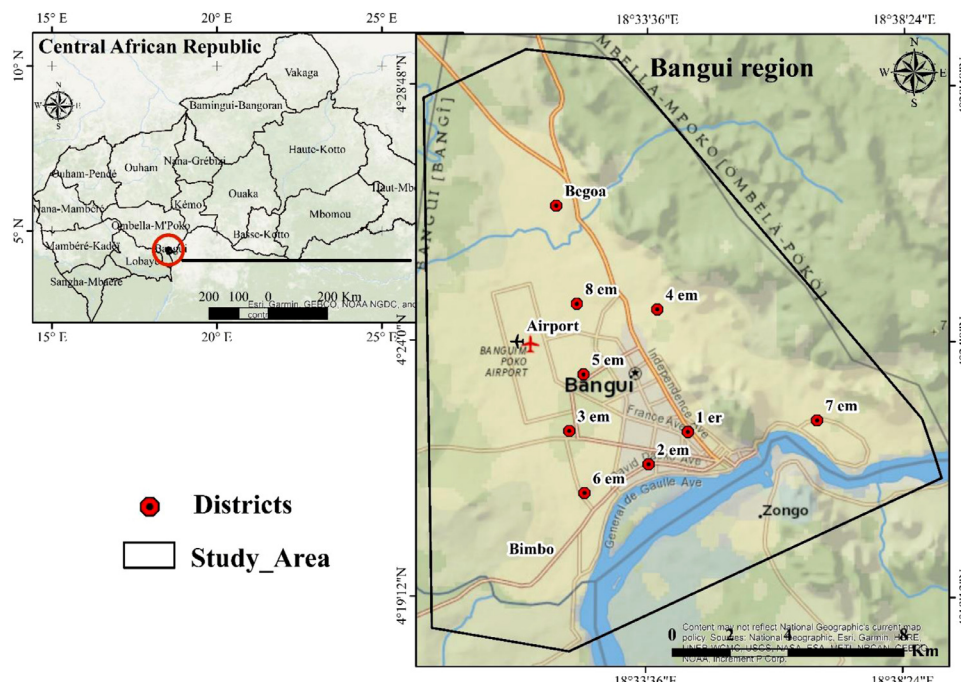


Fig. 1. Map of the study area.

According to an estimate, it is considered that the number of people living in the global metropolitan regions is expected to increase ~ 80% from 2010 to 2050 (Mitchell and Moss, 2012). Central African Republic is one of those countries where urbanization has grown largely in major cities due to a lack of planning and policies. Moreover, an increase in the urban population demands different infrastructures and facilities for their livings, including the construction of new residential and commercial areas, public utility and road infrastructures which ultimately leaving footprints on the eco-environment. In recent years, urbanization has been rapidly increasing in Bangui city because the migration of people from different parts of Central African Republic to the city due to political instability. In addition to this security, all major administrations and major schools and even universities are in this city. This rapid increase of population in the city has been affecting the per-urban economy because of the absorption of farmland and forest cover with impervious surfaces and this also warming the environment of the city and its surrounding. Therefore, accurate, consistent, and updated information on the trend of urbanization is crucial for analysis and policy formulation to ensure a sustainable urban environment in the city.

Over time, land-use change maps provide essential information for land-use planning (Moghadam and Helbich, 2013; Sisay and Korme, 2019) that can help to understand the drivers and dynamics of LULC transformation and predict the future economic and environmental influences (Alemu et al., 2015; Wu and Zhang, 2012). In this regard, GIS and remote sensing are the appropriate tools for land-cover monitoring, urban/regional planning (Dewan and Yamaguchi, 2009; Thapa and Murayama, 2012), and exploring spatiotemporal changes of LULC from a local to a global scale (Ranagalage et al., 2019; Sisay and Korme, 2019; Balew and Korme, 2020). Different techniques can be used to monitor LULC changes, however, the remote sensing method is very significant because it is efficient in covering a wide area, minimize the time and money required for the work. Thus, satellite images such as Landsat are commonly used for environmental monitoring particularly to analyze the impact of LULC change on the variation of LST (Dissanayake et al., 2019b; Priyankara et al., 2019; Balew and Korme, 2020).

Though several studies have been done in different regions of the world, yet the problem of urban climate change mainly SUHI effects is the burning issue of world cities. This initiate to conduct the study and to provide information for city planners about LULC change and its

impact on LST. The study has the objective to examine the impacts of LULC changes on LST in Bangui city from 1986 to 2017 using Landsat images. Therefore, the study is very essential for city planners, municipality experts, as well as other higher officials since the results of the study provide significant information about the trend of LULC change and its impact on LST and enable to implement SUHI mitigation measures.

2. Material and methods

2.1. Study area

Geographically, Bangui city is located in between $4^{\circ} 18' 9''$ N to $4^{\circ} 29' 28''$ N and $18^{\circ} 29' 25''$ E to $18^{\circ} 39' 8''$ E (Fig. 1). It is found in the southern part of Central African Republic (CAR) and in northern Oubangui river bank, which is the border between the Central African Republic and the Democratic Republic of Congo. Bangui is the capital and the largest city of the country with an estimated population of 1.5 million. Bangui city has a tropical climate, in which summers have much more rain when compared with winter. The average temperature of Bangui city is 25.9°C and March is the hottest month in the city, which often reaches up to 40°C . The average rainfall of the city is about 1525 mm per annum.

2.2. Data collection and preprocessing

This study analyzes the impact of LULC change on LST in Bangui city from 1986 to 2017. Different Landsat Products (Landsat 5 (Thematic Mapper (TM)) and Landsat 8 (Operational Land Imager (OLI))) were collected on the temporal resolution of 16 days and spatial resolution of 30 m for the period of 1986, 1999 and 2017 (Table 1). To obtain cloud free Landsat image, image acquired on 16 January 1986, 5 February 1999 and 5 January 2017 were used for the study. All images were freely downloaded from the United States Geological Survey (USGS) earth explorer website (<http://earthexplorer.usgs.gov/>). After the geometric and atmospheric corrections have done (Balew and Korme, 2020; Mumtaz et al., 2020) Landsat products with different spectral bands were mosaicked, layer stacked and processed (Sultana and Satyanarayana, 2018), then spectral bands were employed to derive the LST (Qin et al., 2001a; Jiménez-Muñoz and Sobrino, 2003). To derive

Table 1

The characteristics of the Landsat 5 TM and Landsat 8 OLI.

Band	Landsat 5 TM			Landsat 8 OLI			
	Description	Wavelength (μm)	Resolution (m)	Band	Description	Wavelength (μm)	Resolution (m)
Band1	Blue	0.45–0.52	30	Band1	Coastal/Aerosol	0.433–0.453	30
Band2	Green	0.53–0.61		Band2	Blue	0.450–0.515	
Band3	Red	0.63–0.69		Band3	Green	0.525–0.600	
Band4	Near Infrared	0.78–0.90		Band4	Red	0.630–0.680	
Band5	Short-wave Infrared	1.55–1.75		Band5	Near Infrared	0.845–0.885	
Band7	Short-wave Infrared	2.09–2.35		Band6	Short-wave Infrared	1.560–1.660	
Band6	Thermal Infrared	10.4–12.5	60	Band7	Short-wave Infrared	2.100–2.300	
Image using in this research	Path/Row	Date of acquisition	Source	Band8	Panchromatic	1.360–1.390	15
	181/057	16/01/1986 and 05/02/1999	USGS	Band9	Cirrus	0.52–0.90	30
				Band10	Thermal Infrared	10.6–11.19	100
				Band11	Thermal Infrared	11.5–12.51	
					Path/Row	Date of acquisition	Source
					181/057	05/01/2017	USGS

Table 2

LULC classes and their aerial coverage in Bangui city from 1986 to 2017.

LULC classes	1986			1999			2017		
	Count	Area (km^2)	%	Count	Area (km^2)	%	Count	Area (km^2)	%
Built Up	36,234	32.61	13.22	38,224	34.40	13.95	83443	75.10	30.45
Vegetation	70,252	63.23	25.64	85,639	77.08	31.25	76178	68.56	27.80
Bare soil/rock	151,908	136.72	55.44	134,609	121.15	49.12	98232	88.41	35.85
Water	15,634	14.07	5.71	15,556	14.00	5.68	16175	14.56	5.90
Total	274,028	246.63	100	274,028	246.63	100	274028	246.63	100

LST, firstly the digital numbers of spectral bands were converted into radiance and finally into a brightness temperature value. The detailed procedures for the derivation of radiance and reflectance are explained below. Further, all layer stack spectral bands were also employed to prepare LULC maps of the study area by using a maximum likelihood classifier. These digital image processing were done in ENVI environment while ArcGIS was used for mapping.

2.2.1. Conversion of digital number into radiance

The Landsat images were downloaded as raw data (digital numbers) which needs to be converted to spectral radiances (L_λ) by using the information in the Landsat metadata header file (Mumtaz et al., 2020).

$$L_\lambda = \frac{L_{MAX_\lambda} - L_{MIN_\lambda}}{(Q_{calmax} - Q_{calmin})} \times (Q_{cal} - Q_{calmin}) + L_{MIN_\lambda} \quad (1)$$

Where: L_λ is the spectral radiance ($\text{W m}^{-2} \text{sr}^{-1} \mu\text{m}^{-1}$), L_{MAX_λ} is the spectral radiance scaled to Q_{Calmax} ($\text{W m}^{-2} \text{sr}^{-1} \mu\text{m}^{-1}$). L_{MIN_λ} is the spectral radiance scaled to Q_{Calmin} ($\text{W m}^{-2} \text{sr}^{-1} \mu\text{m}^{-1}$). Q_{Calmax} is the maximum quantized calibrated pixel value (DN = 255) that corresponds to L_{MAX_λ} . The minimum quantized calibrated pixel value (DN = 0) corresponds to L_{MIN_λ} . Q_{Cal} is the quantized calibrated pixel value (DN).

2.2.2. Conversion from radiance to reflectance

The radiances calculated using Eq. (1) were converted into reflectance using Eq. (2) (Chander et al., 2009).

$$r = \frac{\pi \times L_\lambda \times r^2}{E_{sun} \times Cost \times dr} \quad (2)$$

Where: r is the planetary reflectance (dimensionless), L_λ is the spectral radiance at the sensor aperture ($\text{W m}^{-2} \text{sr}^{-1} \mu\text{m}^{-1}$), $dr = 1 + 0.033\cos(D \times 2 \times 3.14)/365$, where D is the day of the year, E_{sun} is the mean solar atmospheric irradiance ($\text{W m}^{-2} \mu\text{m}^{-1}$), θ is the solar zenith angle (degree), $\theta = (90 - B)$, and B is the Sun elevation angle. dr is the inverse square of the earth-sun distance (astronomical unit).

2.2.3. Retrieval Land Surface Temperature (LST)

In this study, LST was derived from thermal bands of Landsat products using the methodology recommended by (Sekertekin et al., 2016). The following procedures were adapted to retrieve LST. In the first step, the radiance of the thermal spectral band retrieved in the previous section was converted into brightness temperature (TB) using the following equation.

$$TB = \frac{K_2}{\ln \left[\left(\frac{K_1}{L_\lambda} \right) + 1 \right]} \quad (3)$$

Where: K_1 and K_2 are the conversions constant, L_λ is a spectral radiance and T is brightness temperature. For Landsat 8 OLI, $K_1 = 774.8853$ Kelvin and $K_2 = 1321.0789$ Kelvin; for Landsat 7 ETM+, $K_1 = 666.09$ Kelvin and $K_2 = 1282.71$ Kelvin; and Landsat 5 TM, $K_1 = 607.76$ Kelvin and $K_2 = 1260.56$ Kelvin.

In the second step, LST was derived using the following relation (Bhalli et al., 2012).

$$LST = \frac{T_B}{1 + \left(\frac{\lambda T_B}{\rho} \right) \ln \epsilon} \quad (4)$$

Where: λ ($\approx 11.5 \mu\text{m}$) is the effective wavelength of thermal bands. $P = \frac{hc}{\lambda^3} = 1.438 \times 10^{-2} \text{ mK}$, where ' σ ' is the Boltzmann constant ($1.38 \times 10^{-23} \text{ J K}^{-1}$), h is Planck constant ($6.626 \times 10^{-34} \text{ Js}$) and c is the speed of light ($3.0 \times 10^8 \text{ ms}^{-1}$), ϵ is the land surface emissivity with 0.95, 0.92 and 0.9925 for vegetation, build-up and water surfaces, respectively (Nichol, 1994). Land surface emissivity (ϵ) was estimated using the NDVI thresholds method as proposed by (Jiménez-Muñoz and Sotelo, 2003), according to the following equation.

$$\epsilon = (1 - \epsilon_s) \times (1 - p_v) + F \times \epsilon_V \quad (5)$$

Where: d_ϵ = geometrical distribution of the surface; ϵ_v = vegetation emissivity; ϵ_s = the soil emissivity; F = shape factor and its value is 0.55; p_v = vegetation proportion and it was obtained according to Eq. 6 (Bhalli et al., 2012; Sisay and Korme, 2019; Balew and Ko-

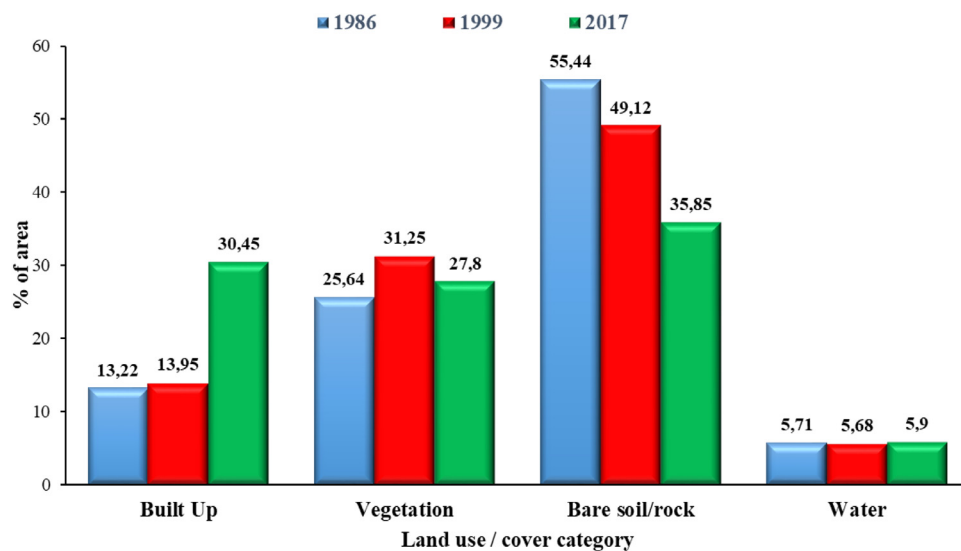


Fig. 2. Graphical representation of the area of LULC classes of Bangui city from 1986 to 2017.

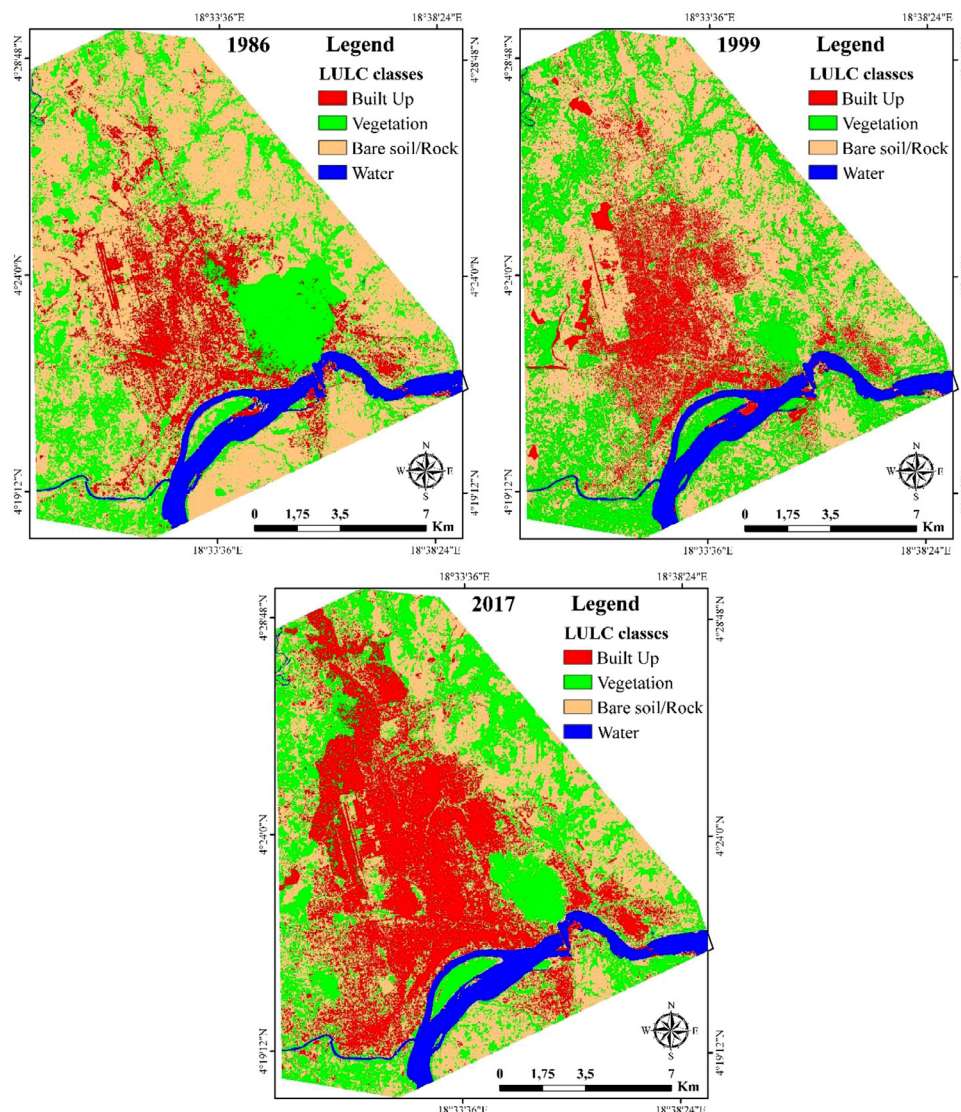


Fig. 3. LULC map of Bangui city in 1986, 1999 and 2017.

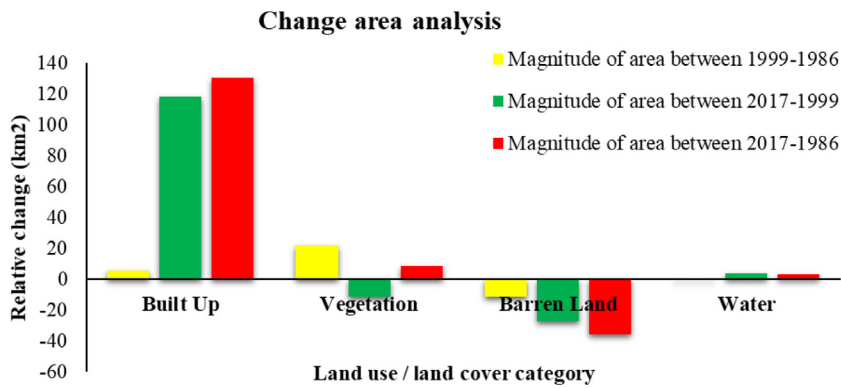


Fig. 4. Graphical representation of LULC change in Bangui city during 1986–2017.

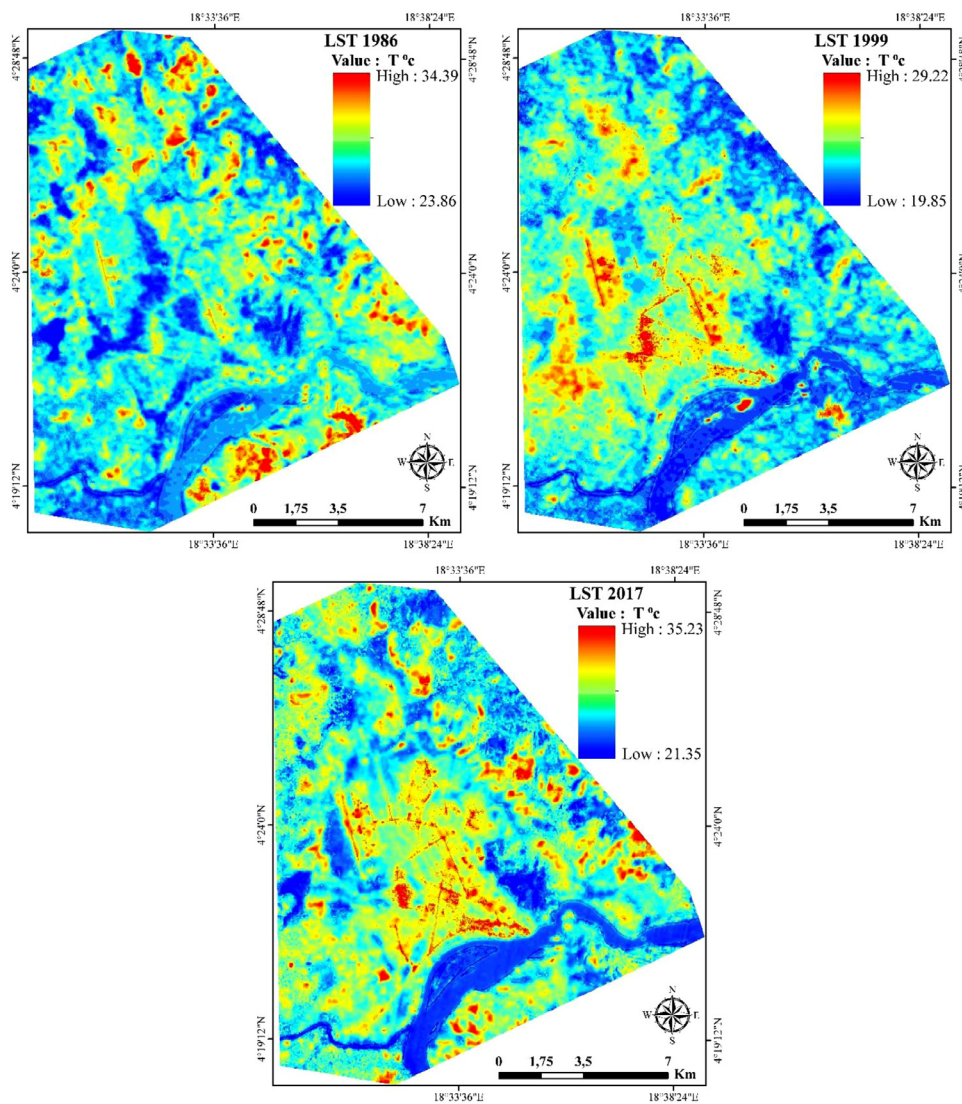


Fig. 5. LST map of Bangui city in 1986, 1999 and 2017.

rme, 2020).

$$P_v = \left(\frac{NDVI - NDVI_{min}}{NDVI_{max} - NDVI_{min}} \right)^2 \quad (6)$$

Then land surface emissivity was retrieved using equation 7.

$$\epsilon = (\epsilon_s \times P_v) + \epsilon_s (1 - p_v) + d_\epsilon \quad (7)$$

2.2.4. Calculation of spectral indices

The NDVI is widely used as the vegetation indicator by combining the reflectance of two-channels which sensitive to vegetation feature, including red band (RED) and near-infrared band (NIR). The NDVI ranges from -1 to +1. The NDVI is expressed in the following equation (Simwanda and Murayama, 2018; Sisay and Korme, 2019; Balew and Korme, 2020).

$$NDVI = \frac{\rho_{Red} - \rho_{Nir}}{\rho_{Red} + \rho_{Nir}} \quad (8)$$

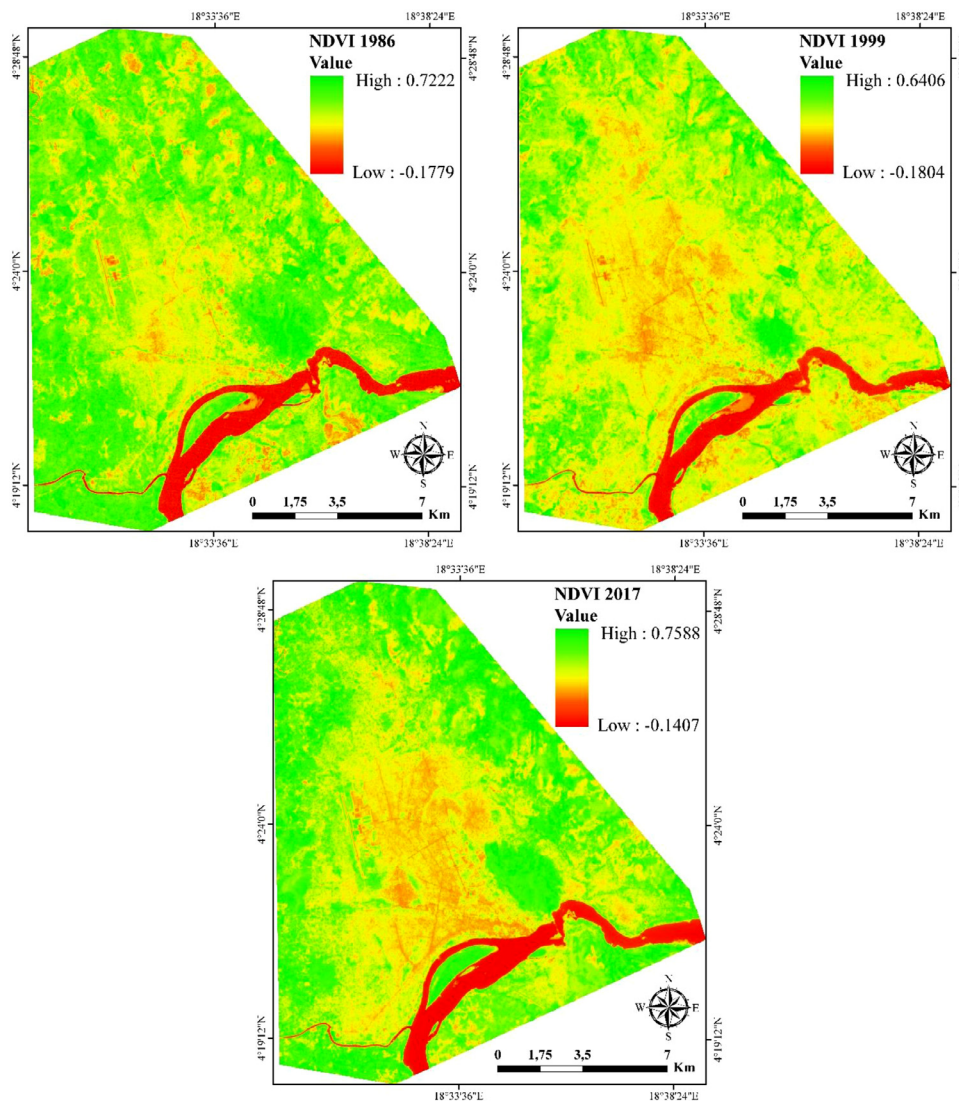


Fig. 6. NDVI of Bangui city for 1986, 1999, and 2017.

Where: ρ_{red} and ρ_{Nir} correspond to the reflectance of Red and Near-infrared bands of Landsat images, respectively.

The NDBI is also an effective technique for characterizing information of built-up features. It is calculated based on the difference between NIR and MIR bands. The NDBI is expressed in the following equations.

$$NDBI = \frac{\rho_{Mir} - \rho_{Nir}}{\rho_{Mir} + \rho_{Nir}} \quad (9)$$

Where: ρ_{Mir} and ρ_{Nir} correspond to the reflectance of Middle-infrared and Near-infrared bands of Landsat images, respectively.

The NDLI has been proven as an effective indicator in assessing the potential evapotranspiration of the surface. The advantage of the NDLI is its uniqueness in optimizing the spectral sensitivity on biophysical land surface parameters by incorporating three commonly channels chosen by the satellite missions, including Green, Red, and Shortwave-infrared. The NDLI is estimated by the equation below.

$$NDLI = \frac{\rho_{Green} - \rho_{Red}}{\rho_{Green} + \rho_{Red} + \rho_{Mir}} \quad (10)$$

Where: ρ_{Green} , ρ_{Red} and, ρ_{Mir} correspond to the reflectance of Green, Red, and Near-infrared bands of Landsat images, respectively.

2.3. Preparation of land use/land-cover classes

After radiance was converted to reflectance in Eq. 2, LULC classes were extracted for the period 1986, 1999 and 2017 by applying maxi-

mum likelihood supervised classification. Supervised classification was used to classify the pixels into different land use classes (Asmala, 2012). The LULC classes of the study area were categorized into four classes: vegetation, water bodies, built-up and bare soil/rock.

2.4. Statistical analysis

The study used Correlation coefficient (R) to assess the relationship between LST and NDVI, NDBI and NDLI of the study area of each year. The study was used three indices namely NDVI, NDBI and NDLI to characterize the surface and LST variations in Bangui city. These indices were used to establish quantifiable relationships with LST through the set of independent pixels chosen randomly within the entire study area. The statistical relationship was implemented using the Excel 2016 software package.

3. Results and discussion

3.1. Land-use/land-cover change from 1986 to 2017

Built up, vegetation, bare soil/ rock and water were the main LULC types found in Bangui city. The spatiotemporal distribution of LULC classes of the city in 1986, 1999 and 2017 are illustrated in Fig. 3. Table 2 and Fig. 2 also shows the statistical information of LULC classes found in the city. In 1986, bare soil/rock was the largest LULC class

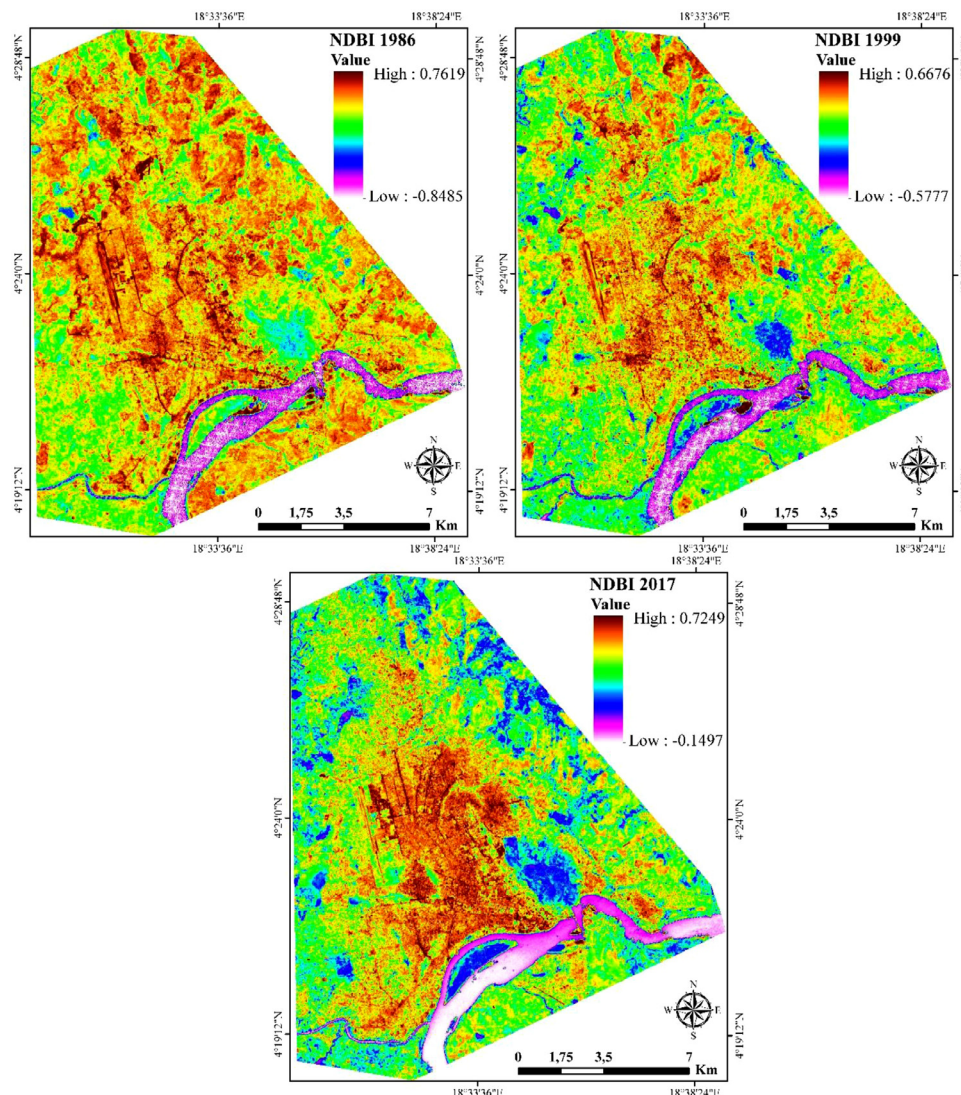


Fig. 7. NDBI of Bangui city for 1986, 1999, and 2017.

Table 3
LULC changes in Bangui city from 1986 to 2017.

LULC Class	1999-1986			2017-1999			2017-1986		
	Area (km ²)	% Change	Rate	Area (km ²)	% Change	Rate	Area (km ²)	% Change	Rate
Built Up	1.791	5.49	13.78	40.70	118.30	657.22	42.49	130.29	137.06
Vegetation	13.8483	21.90	106.53	-8.51	-11.05	-61.38	5.33	8.44	17.20
Bare Soil/rock	-15.569	-11.39	-119.76	-32.74	-27.02	-150.1	-48.31	-35.33	-155.83
Water	-0.0702	-0.50	-0.54	0.56	3.98	22.11	0.49	3.46	1.57

which was occupied an area of 136.72 km² (55.44%), followed by vegetation (63.23 km² or 25.64%). The remaining area of the city was covered with built-up (32.61 km²) and water (14.07 km²). Bare soil/rock was also the dominant class in 1999 thought it declined to 121.15 km² from 1986. On the contrary, vegetation covers slightly increased to 77.08 km² (31.25%). Built-up areas increased from 1986 to 1999 with an increase of 1.79 km² and 0.07 km² of the water body was converted to other LULC types. During 2017, the built-up area was highly expanded and cover an area 75.1 km² (30.45%). Whereas vegetation cover and bare soil/rock were declined to 68.56 km² (27.8%) and 88.41 km² (35.85%) respectively when it compares in 1999. The water body increased to 14.56 km² (5.9%) (Table 2).

The result of the study shows that there was a small increase in built-up areas (5.46%) from 1986 to 1999 (Table 3 and Fig. 4). Vegetation

cover also increased (21.9%) from 1986 to 1999 whereas -11.39% and -0.5% of bare soil and water were decreased and converted to other LULC types respectively. Furthermore, between 1999 and 2017, we observed a strong increase in built-up areas (118.3%), and water body (3.98%). However, in the same period, we observed a decrease in the area of bare soil/rock (-27.02%) and vegetation (-11.05%). The result also indicates that there was a significant change in LULC between 1986 and 2017. For instance, built-up increased by +130.29 % with a rate of 137.06. Vegetation also increased by 8.44% or a rate of 17.2 and a slight increase in water body by 3.46% with a rate of 1.57. Nonetheless, bare soil/rock recorded a sharply declined by -35.33% for a rate of -155.83. Therefore, the study revealed that there was a LULC transformation that varies within time and space. This change is mostly attributed to rapid urbanization. The study is in line with for-

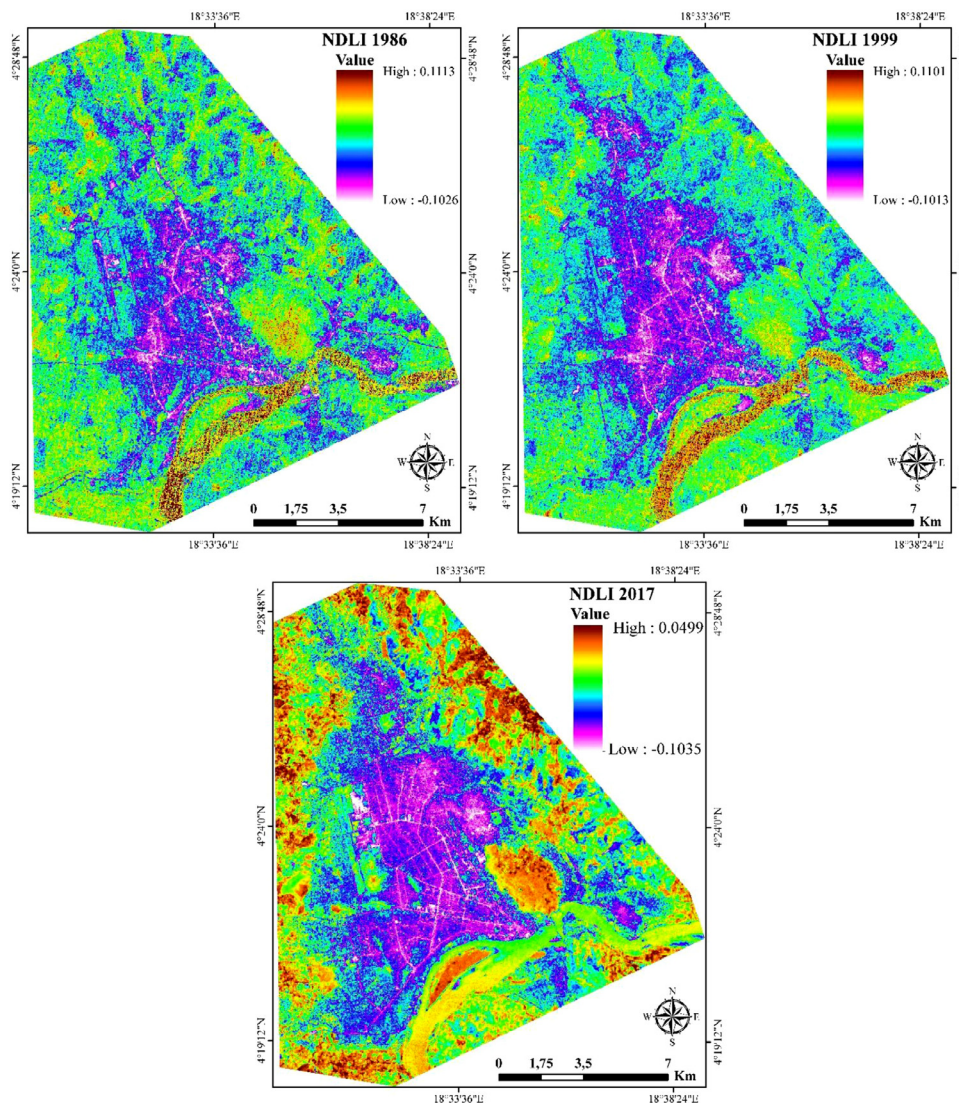


Fig. 8. NDLI of Bangui city for 1986, 1999, and 2017.

mer research findings (Arsiso et al., 2018; Mohamed and Worku, 2019; Priyankara et al., 2019; Simwanda et al., 2019; Sisay and Korme, 2019; Balew and Korme, 2020; Vani and Prasad, 2020). Extreme land transformation contributes to different environmental problems of urban areas such as SUHI.

3.2. Spatiotemporal distribution of LST and its variations with LULC types

Fig. 5 shows the spatial distributions of LST for three study periods (1986, 1999, and 2017). The result shows that the minimum and maximum LST of the city on 16 January 1986 were 23.86 °C and 34.39 °C respectively. However, on 5 February 1999, the minimum and maximum LST values were 19.85 °C and 29.22 °C respectively. On 5 January 2017, the minimum LST raised to 21.35 °C and a maximum of 35.23 °C. The mean LST values of the city were 26.24 °C, 23.37 °C and 27.23 °C respectively in 1986, 1999 and 2017 (Table 4).

The study confirmed that central areas of the city were exhibited high LST and it declined when moving away from the center. This is because of buildings and other impervious surface expansion (Dissanayake et al., 2019a, 2019b; Ranagalage et al., 2019; Simwanda et al., 2019; Sisay and Korme, 2019; Vani and Prasad, 2020). The result also indicates that the highest LST in all three study periods corresponds to dry features with the appearance of impervious, rock,

Table 4
Mean LST of LULC types of Bangui city in 1986, 1999 and 2017.

Mean LST (°C)	1986	1999	2017
Whole area	26.24	23.37	27.23
Built-up	26.21	23.92	27.59
Bare soil & Rock	26.51	23.55	27.33
Vegetation	25.56	23.02	26.92
Water body	25.06	23.03	25.64

and bare soil surfaces. These features increased the efficiency of the surface in solar energy absorption and transformed into heat energy (Qin et al., 2001a; Liu et al., 2015; Qijiao and Zhixiang, 2015). Therefore, it increased the temperature of the land surface. For instance, crowded residential areas and other infrastructures in the city centers formed high LST compared to surrounding areas in 1999 and 2017. The mean LST values of built-up areas in 1999 and 2017 were 23.92 °C and 27.59 °C respectively whereas in 1986 it was 26.21 °C (Table 4). The mean LST values of bare soil in the city were 26.51 °C, 23.55 °C and 27.33 °C in 1986, 1999 and 2017 respectively. While lower LST concentrated in areas where high vegetation cover was found mainly along the dense forest in the eastern and southwestern part of the city. Low LST was also found in places along the Oubangui River and its surrounding.

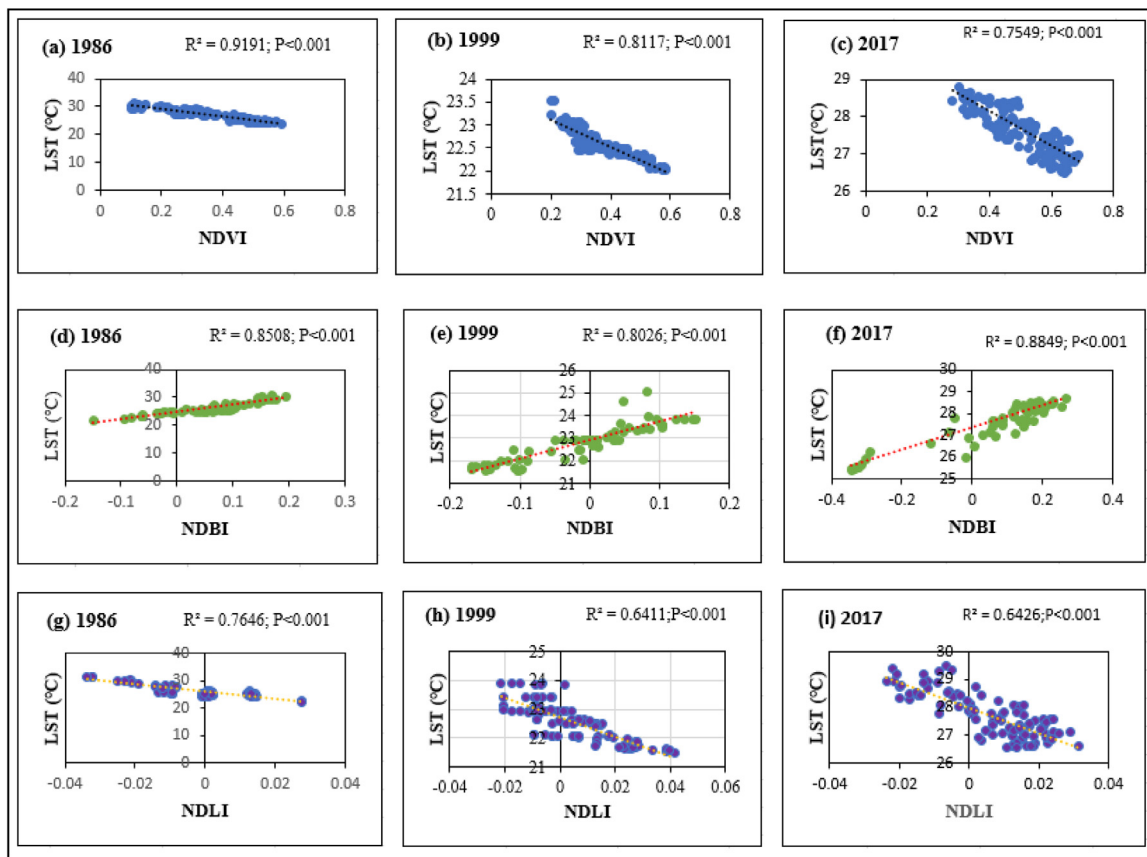


Fig. 9. Correlation between LST and NDVI (a-c), LST and NDBI (d-f), LST and NDLI (g-i).

For example, the mean LST values of water body increased from 25.06 °C in 1986 to 25.64 °C in 2017 though it was 23.03 °C in 1999. Similar to water body, the mean LST of vegetation cover decreased from 25.56 °C in 1986 to 23.02 °C in 1999 and increased to 26.92 °C in 2017. This is because vegetation leave and canopy absorb radiation and regulate the energy of the surrounding environment. Hence, this finding is similar to other research findings (Elmes et al., 2017; Peng et al., 2014; Sisay and Korme, 2019; Balew and Korme, 2020). Thus, the transformation of land-cover types to land-use due to rapid urbanization increase LST (Dissanayake et al., 2019a; Simwanda and Murayama, 2018; Ranagalage et al., 2019; Simwanda et al., 2019; Sisay and Korme, 2019; Balew and Korme, 2020; Vani and Prasad, 2020).

3.3. Relationship of LST with NDVI, NDBI and NDLI

The study revealed that most places in the center of the city exhibited low NDVI values while peripheral areas and places covered with vegetation have high NDVI values (Fig. 6). This indicates that NDVI is inversely related to LST since the central place has high LST values. Therefore, it is inversely correlated with LST. On the other hand, NDBI was very high in the center of the city and some places which are directly exposed to the incoming solar radiation such as bare soil/rock and these places have high LST (Fig. 7). Therefore, the result of this study is in line with previous findings (Sisay and Korme, 2019; Balew and Korme, 2020). The NDLI was low in the center of the city mainly built-up areas and high along with the waterbody and vegetation cover (Fig. 8).

The result of this study shows that there is a negative correlation between LST and NDVI ($r = -0.9191, -0.8117$, and -0.7549 for 1986, 1999, and 2017, respectively) (Fig. 9a-c). However, the study confirmed that the correlation coefficient between LST and NDBI was positive with the values of $r = 0.8508$, 0.8026 , and 0.8849 for 1986, 1999, and 2017, respectively (Fig. 9d-f). That means urbanization has a great impact on the surface thermal environment. The study also found a strong negative

correlation between NDLI and LST with a coefficient of $r = -0.7646$, 0.6411 , and 0.6426 for 1986, 1999, and 2017, respectively (Fig. 9g-i). It means that the high value of LST corresponds to low surface water availability and vice versa. Hence, it is in line with the fact that water availability increases the amount of water transfer from the land to the atmosphere through evapotranspiration which can actually reduce the surface temperature. Thus, the result of the current study agree with previous research findings (Liou and Mulualem, 2019).

4. Conclusions

Land-cover types has been degraded from time to time and this degradation cause change in urban climate. Continuous and extreme land and environmental degradation, particularly affect LST in many cities in the world. So, monitoring LULC is very vital to understand trend of LST. In this regards, advanced remote sensing technology has been used for environmental resource monitoring and planning. The result of the study indicates that built-up areas were expanded from 1986 to 2017 whereas bare soil declined. Besides, the area of vegetation cover was somewhat increased from 1986 to 2017 due to the expansion of green space in the city. Though green areas were expanded in the city, the LST increasing from 1986 to 2017. The study revealed that the minimum, maximum and mean LST of the city increased during the study period. The study also stated that built-up and bare soil experienced higher LST than vegetation and water body. This study indicates that significant variations of LST related to the transformation of LULC in Bangui city originating from the urbanization process. The study found a positive correlation between NDBI and LST whereas negative correlations between LST and NDVI and NDLI. Therefore, to mitigate the impact of LULC change on LST the city planner and administrator should work on different landscape planning on ecological and biodiversity perspectives. The landscape planning of the city should also focus on the techniques of regulating the effects of SUHI. The city administra-

tor should also work to increase urban green belts and green roof mechanisms.

Declaration of Competing Interest

We declare that there is no conflict of interest between authors.

Ethical approval and consent to participate

Not applicable.

Consent of publication

Not applicable.

Authors' contributions

MT prepared the research proposal, acquire Landsat images and process and interpret the data and writing research draft and the manuscript. MSL participated in analyzing and investigating the methods and editing the manuscript. AR interpreted the data and prepared the manuscript for publication. AB prepared the graphs and preparing and editing the manuscript. Both authors edit and revised the manuscript and approved it to send to the journal.

Funding

Not applicable.

Available of data and materials

All data generated or analyzed during this study are included in this published article [and its supplementary information files].

References

- Abdullahi, S., Pradhan, B., 2018. Land use change modeling and the effect of compact city paradigms: integration of GIS-based cellular automata and weights-of-evidence techniques. *Environ. Earth Sci.* 77, 251.
- Aleme, B., Garedew, E., Eshetu, Z., Kassa, H., 2015. Land use and land cover changes and associated driving forces in north western lowlands of Ethiopia. *Int. Res. J. Agric. Sci. Soil Sci.* 5, 28–44.
- Arsiso, B.K., Tsidu, G.M., Gerrit, H.S., Tadesse, T., 2018. Influence of urbanization-driven land use/cover change on climate: the case of Addis Ababa, Ethiopia. *Phys. Chem. Earth*, 105, 212–223.
- Asmala, A., 2012. Analysis of maximum likelihood classification on multispectral data. *Appl. Math. Sci.* 6, 6425–6436.
- Balew, A., Korme, T., 2020. Monitoring land surface temperature in Bahir Dar City and its surrounding using Landsat images. *Egypt J. Remote Sens. Space Sci.* 23, 371–386.
- Bhalli, M.N., Ghaffar, A., Shirazi, S.A., Parveen, N., Anwar, M.M., 2012. Change detection analysis of land use by using geospatial techniques: a case study of Faisalabad-Pakistan. *Sci. Int.* 24, 539–546.
- Bounoua, L., Nigro, J., Zhang, P., Thome, K., Lachir, A., 2018. Mapping urbanization in the United States from 2001 to 2011. *Appl. Geogr.* 90, 123–133.
- Chander, G., Markham, B.L., Helder, D.L., 2009. Summary of current radiometric calibration coefficients for Landsat MSS, TM, ETM+, and EO-1 ALI sensors. *Remote Sens. Environ.* 113, 893–903.
- Chen, X.L., Zhao, H., Li, P., Yin, Z., 2006. Remote sensing image-based analysis of the relationship between urban heat island and land use/cover changes. *Remote Sens. Environ.* 104, 133–146.
- Dewan, A.M., Yamaguchi, Y., 2009. Using remote sensing and GIS to detect and monitor land use and land cover change in Dhaka Metropolitan of Bangladesh during 1960–2005. *Environ. Monit. Assess.* 150, 237.
- Dissanayake, D., Morimoto, T., Murayama, Y., Ranagalage, M., 2019a. Impact of landscape structure on the variation of land surface temperature in sub-saharan region: a case study of Addis Ababa using Landsat data (1986–2016). *Sustainability* 11.
- Dissanayake, D., Morimoto, T., Ranagalage, M., Murayama, Y., 2019b. Land-use/land-cover changes and their impact on surface urban heat islands: case study of Kandy City, Sri Lanka. *Climate* 7.
- Dubovyk, O., Sliuzas, R., Flacke, J., 2011. Spatio-temporal modelling of informal settlement development in Sancaktepe district, Istanbul, Turkey. *ISPRS J. Photogramm. Remote Sens.* 66, 235–246.
- Elmes, A., Rogan, J., Williams, C., Ratnick, S., Nowak, D., Martin, D., 2017. Effects of urban tree canopy loss on land surface temperature magnitude and timing. *ISPRS J. Photogramm. Remote Sens.* 128, 338–353.
- Jiménez-Muñoz, J.C., Sobrino, J.A., 2003. A generalized single-channel method for retrieving land surface temperature from remote sensing data. *J. Geophys. Res.* 108.
- Kalnay, E., Cai, M., 2003. Impact of urbanization and land-use change on climate. *Nature* 423, 528 2003.
- Liou, Y.-A., Muluaalem, G.M., 2019. Spatio-temporal assessment of drought in Ethiopia and the impact of recent intense droughts. *Remote Sens.* 11, 1828.
- Liu, K., Su, H., Li, X., Wang, W., Yang, L., Liang, H., 2015. Quantifying spatial-temporal pattern of urban heat Island in Beijing: an improved assessment using land surface temperature (LST) time series observations from LANDSAT, MODIS, and Chinese New Satellite GaoFen-1. *IEEE J. Sel. Top. Appl. Earth Obs. Remote Sens.*
- Lu, Q., Chang, N.-B., Joyce, J., Chen, A.S., Savic, D.A., Djordjevic, S., Fu, G., 2018. Exploring the potential climate change impact on urban growth in London by a cellular automata-based Markov chain model. *Comput. Environ. Urban Syst.* 68, 121–132.
- Lu, Y., Wu, P., Ma, X., Li, X., 2019. Detection and prediction of land use/land cover change using spatiotemporal data fusion and the Cellular Automata–Markov model. *Environ. Monit. Assess.* 191, 68.
- Mitchell, L., and Moss, H.O.N. (2012). Urban Mobility in the 1st Century.
- Moghadam, H.S., Helbich, M., 2013. Spatiotemporal urbanization processes in the megacity of Mumbai, India: a Markov chains-cellular automata urban growth model. *Appl. Geogr.* 40, 140–149.
- Mohamed, A., Worku, H., 2019. Quantification of the land use/land cover dynamics and the degree of urban growth goodness for sustainable urban land use planning in Addis Ababa and the surrounding Oromia special zone. *J. Urban Manag.* 8, 145–158.
- Mumtaz, F., 2020. The relationship between vegetation dynamics and land surface temperature by using different satellite imageries; A case study of Metropolitan cities of Pakistan. *N. Am. Acad. Res.* 3, 1–15.
- Mumtaz, F., Tao, Y., de Leeuw, G., Zhao, L., Fan, C., Elnashar, A., Bashir, B., Wang, G., Li, L., Naeem, S., et al., 2020. Modeling spatio-temporal land transformation and its associated impacts on land surface temperature (LST). *Remote Sens.* 12, 2987.
- Nichol, J.E., 1994. A GIS-based approach to microclimatic monitoring in Singapore's high-rise housing estates. *Photogramm. Eng. Remote Sens.* 60, 1225–1232.
- Omar, N.Q., Sanusi, S.A.M., Hussin, W.M.W., Samat, N., Mohammed, K.S., 2014. Markov-CA model using analytical hierarchy process and multiregression technique. *7th IGRSM International Remote Sensing & GIS Conference and Exhibition*, (in IOP Conference Series: Earth and Environmental Science. IOP Publishing.
- Peng, S.S., Piao, S., Zeng, Z., Ciais, P., Zhou, L., Li, L.Z., Myneni, R.B., Yin, Y., Zeng, H., 2014. Afforestation in China cools local land surface temperature. *Proc. Natl. Acad. Sci. USA* 2915–2919.
- Poelmans, L., Van Rompaey, A., 2009. Detecting and modelling spatial patterns of urban sprawl in highly fragmented areas: a case study in the Flanders–Brussels region. *Landsc. Urban Plan.* 93, 10–19.
- Priyankara, P., Ranagalage, M., Dissanayake, D., Morimoto, T., Murayama, Y., 2019. Spatial process of surface urban heat island in rapidly growing seoul metropolitan area for sustainable urban planning using landsat data (1996–2017). *Climate* 7.
- Qijiao, X., Zhixiang, Z., 2015. Impact of urbanization on urban heat island effect based on TM imagery in Wuhan, China. *Environ. Eng. Manag. J.* 14, 647–655.
- Qin, Z., Karnieli, A., Berliner, P., 2001a. A mono-window algorithm for retrieving land surface temperature from Landsat TM data and its application to the Israel-Egypt border region. *Int. J. Remote Sens.* 21, 3719–3746.
- Rajeshwari, A., Mani, N.D., 2014. Estimation of land surface temperature of dindigul district using landsat 8 data. *Int. J. Res. Eng. Technol.* 3, 122–126.
- Ranagalage, M., Murayama, Y., Dissanayake, D., Simiwanda, M., 2019. The impacts of landscape changes on annual mean land surface temperature in the tropical mountain city of Sri Lanka: a case study of Nuwara Eliya (1996–2017). *Sustainability* 11.
- Sekertekin, A., Kutoglu, S.H., Kaya, S., 2016. Evaluation of spatio-temporal variability in land surface temperature: a case study of Zonguldak, Turkey. *Environ. Monit. Assess.* 188, 30.
- Seto, K.C., Fragiadakis, M., Guneralp, B., Reilly, M.K., 2011. A meta-analysis of global urban land expansion. *PLoS One* 6.
- Simwanda, M., Murayama, Y., 2018. Spatiotemporal patterns of urban land use change in the rapidly growing city of Lusaka, Zambia: implications for sustainable urban development. *Sustain. Cities Soc.* 39, 262–274.
- Simwanda, M., Ranagalage, M., Estoque, R.C., Murayama, Y., 2019. Spatial analysis of surface urban heat islands in four rapidly growing African cities. *Remote Sens.* 11.
- Sisay, D.C., Korme, T., Toda, 2019. Understanding land surface temperature on rift areas to examine the spatial variation of urban heat island: the case of Hawassa, southern Ethiopia. *GeoJournal*.
- Solaimani, K., Arekhi, M., Tamartash, R., Miryaghobzadeh, M., 2010. Land use/cover change detection based on remote sensing data (A case study; Neka Basin). *Agric. Biol. J. N. Am.* 1, 1148–1157.
- Sultana, S., Satyanarayana, A.N.V., 2018. Urban heat island intensity during winter over metropolitan cities of India using remote-sensing techniques: impact of urbanization. *Int. J. Remote Sens.* 39, 6692–6730.
- Sun, C., Wu, Z., Lv, Z., Yao, N., Wei, J., 2013. Quantifying different types of urban growth and the change dynamic in Guangzhou using multi-temporal remote sensing data. *Int. J. Appl. Earth Obs. Geoinf.* 21, 409–417.
- Thapa, R.B., Murayama, Y., 2012. Scenario based urban growth allocation in Kathmandu Valley, Nepal. *Landsc. Urban Plan.* 105, 140–148.
- Vani, M., Prasad, P.R.C., 2020. Assessment of spatio-temporal changes in land use and land cover, urban sprawl, and land surface temperature in and around Vijayawada city, India. *Environ. Dev. Sustain.* 22, 3079–3095.
- Wu, K.Y., Zhang, H., 2012. Land use dynamics, built-up land expansion patterns, and driving forces analysis of the fast-growing Hangzhou metropolitan area, eastern China (1978–2008). *Appl. Geogr.* 34, 137–145.
- Zhang, R., Matsushima, K., Kobayashi, K., 2018. Can land use planning help mitigate transport-related carbon emissions? A case of Changzhou. *Land Use Policy* 74, 32–40.